International Journal of Heat and Mass Transfer 72 (2014) 352–361

Contents lists available at ScienceDirect

International Journal of Heat and Mass Transfer

journal homepage: www.elsevier.com/locate/ijhmt

Estimation of the local heat-transfer coefficient in the laminar flow regime in coiled tubes by the Tikhonov regularisation method

Fabio Bozzoli [a,1], Luca Cattani [a,1], Sara Rainieri [a,b,*], Fermín S. Viloche Bazán [c,2], Leonardo S. Borges [d,2]

[a] Department of Industrial Engineering, University of Parma, Parco Area delle Scienze 181/A, I-43124 Parma, Italy
[b] SITEIA.PARMA Interdepartmental Centre, University of Parma, Parco Area delle Scienze 181/A, I-43124 Parma, Italy
[c] Department of Mathematics, Federal University of Santa Catarina, CEP 88040-900, Florianópolis/SC, Brazil
[d] Department of Mathematics, Federal University of Technology, CEP 84016-210, Ponta Grossa/PR, Brazil

ARTICLE INFO

Article history:
Received 31 July 2013
Received in revised form 24 December 2013
Accepted 7 January 2014
Available online 3 February 2014

Keywords:
Heat-transfer enhancement
Coiled tubes
Local convective heat-flux estimation
Inverse heat conduction problem

ABSTRACT

Wall curvature is a widely used technique to passively enhance convective heat transfer that has proven to also be effective in the thermal processing of highly viscous fluids. These geometries produce a highly uneven convective heat-flux distribution at the wall along the circumferential coordinate, thus affecting the performance of the fluid thermal treatment. Although many authors have investigated the forced convective heat transfer in coiled tubes, most of them have presented the results only in terms of the Nusselt number averaged along the wall circumference. A procedure to estimate the local convective wall heat flux in coiled tubes is presented and tested in this paper: the temperature distribution maps on the external coil wall were employed as input data of the inverse heat conduction problem in the wall under a solution approach based on the Tikhonov regularisation method with the support of the fixed-point iteration technique to determine a proper regularisation parameter. The investigation was focused on the laminar flow regime.

1. Introduction

Wall curvature is among the most frequently used passive techniques to enhance convective heat transfer. The effectiveness of wall curvature occurs because it gives origin to the centrifugal force in the fluid: this phenomenon induces local maxima in the velocity distribution that locally increase the temperature gradients at the wall by maximising the heat transfer [1–6]. The asymmetrical distribution of the velocity field over the cross-section of the tube leads to a significant variation in the convective heat-transfer coefficient along the circumferential angular coordinate: it presents higher values at the outer bend side of the wall surface than at the inner bend side.

This irregular distribution may be critical in some industrial applications, such as in those that involve a thermal process. For instance, in food pasteurisation, the irregular temperature field induced by the wall curvature could reduce the bacteria heat-killing or could locally overheat the product. Therefore, to predict the overall performance of heat-transfer apparatuses that involve the use of curved tubes, it is necessary to know the local distribution of the convective heat-transfer coefficient not only along the axis of the heat-transfer section but also at the fluid-wall interface along the cross-section circumference.

Although many authors have investigated the forced convective heat transfer in coiled tubes, most of them have presented the results only in terms of the Nusselt number averaged along the wall circumference: only a few authors have studied the phenomenon locally, and most of them have adopted the numerical approach.

Yang et al. [7] presented a numerical investigation on the fully developed laminar convective heat transfer in a helicoidal pipe, with particular attention to the effects of torsion on the local heat-transfer coefficient. In particular, the authors reported the Nusselt number distribution varying the coil pitch, and they showed that, due to torsion, the local heat-transfer coefficient, compared to the case of an ideal torus, is increased on half of the tube wall while it is decreased on the other half.

Jayakumar et al. [8] numerically analysed the turbulent heat transfer in helically coiled tubes and presented the local Nusselt number at various cross sections along the curvilinear coordinate. The results showed that, on any cross section, the highest Nusselt number is on the outer side of the coil, and the lowest one is expected on the inner side. Moreover, the authors proposed a correlation for predicting the

* Corresponding author at: Department of Industrial Engineering, University of Parma, Parco Area delle Scienze 181/A, I-43124 Parma, Italy. Tel.: +39 0521 905857; fax: +39 0521 905705.
E-mail addresses: fabio.bozzoli@unipr.it (F. Bozzoli), luca.cattani@nemo.unipr.it (L. Cattani), sara.rainieri@unipr.it (S. Rainieri), fermin.bazan@ufsc.br (F.S. Viloche Bazán), lsbplsb@yahoo.com (L.S. Borges).
[1] Tel.: +39 0521 905857; fax: +39 0521 905705.
[2] Tel./fax: +55 48 331 9221.

0017-9310/$ - see front matter © 2014 Elsevier Ltd. All rights reserved.
http://dx.doi.org/10.1016/j.ijheatmasstransfer.2014.01.019

Nomenclature

a	coil diameter (m)
D_{int}	tube internal diameter (m)
De	Dean number (–)
h	convective heat-transfer coefficient (W/m^2 K)
g	gravitational acceleration (m/s^2)
Gr	Grashof number $Gr = g \cdot \beta_f \cdot (\overline{T_w} - T_b) \cdot D_{\text{int}}^3 \cdot \rho_f^2/\mu_f^2$ (–)
Nu	Nusselt number (–)
q	convective heat flux (W/m^2)
$\mathbf{q}$	convective heat-flux vector (W/m^2)
q_g	internal heat generation per unit volume (W/m^3)
r	radial coordinate m
Re	Reynolds Number ($Re = w \cdot D_i \cdot \rho_f/\mu_f$) (–)
R_{env}	overall heat-transfer resistance between the tube wall and the surrounding environment (m^2 K/W)
T	temperature (K)
w	mean axial velocity
$\mathbf{X}$	sensitivity matrix (m^2 K/W)
P	coil pitch (m)
α	angular coordinate (rad)
β	volumetric thermal expansion coefficient (K^{-1})
Γ	dimensionless curvature of the coil ($\Gamma = D_{int}/a$)
Π	dimensionless torsion of the coil ($\Pi = P/\pi a$)
k	thermal conductivity (W/m K)
μ	dynamic viscosity (Pa s)
ρ	density (kg/m^3)

Subscripts, superscripts

b	bulk
env	environment
ext	external
f	fluid
int	internal

local Nusselt number as a function of the average Nusselt number and the angular location for both the constant temperature and the constant heat-flux boundary conditions.

Bai et al. [9] experimentally studied the turbulent heat transfer in helically coiled tubes using deionised water as the working fluid. As expected, they found that the local heat-transfer coefficient was not evenly distributed along the periphery of the cross section and that, in particular, at the outside surface of the coil, it was three or four times higher than that at the inside surface.

Bozzoli et al. [10] presented preliminary results regarding the local convective heat coefficient in coiled tubes for the laminar flow regime: because the estimation method proposed in this paper was based on the non-linear inverse heat conduction problem (IHCP), several strong approximations in the formulation of the model were adopted due to the restrictions imposed by the high computational cost of the minimisation algorithm.

To the authors' knowledge, the experimental data presented by Bozzoli et al. [10] are the only data available on the local heat transfer in coiled tubes for the laminar flow regime that is frequently encountered in industrial fields where highly viscous fluids are processed.

As shown by Bozzoli et al. [10], the solution of the IHCP in the wall, starting from the temperature distribution acquired on the external wall surface, is a robust tool to estimate the local convective heat-transfer coefficient on the interior wall surface. However, because IHCPs are generally ill-posed, the solution may not be unique and would have great sensitivity to small variations in the input data. To cope with this difficulty, many techniques have been proposed, and the most well-known are: function specification methods [11,12], iterative methods [13–15], methods based on filtering proprieties [16–18] and regularisation techniques[19,20].

Among the regularisation techniques, Tikhonov regularisation method [20] is perhaps the most common: it promotes the construction of stable approximate solutions to the original IHCP by solving a well-posed problem via the minimisation of an objective function. The objective function is expressed by the sum of the squared difference between the measured and the estimated temperature discrete data and of a regularisation parameter times a term that expresses the smoothness of the unknown quantity. The regularisation scheme suggested by Tikhonov and Arsenin [20] in the case of a particularly critical signal-to-noise ratio makes it possible to overcome the instability of the problem. The success of this approach relies on a proper choice of the regularisation parameter, and this is not an easy task.

The classical L-curve method to select a proper regularisation parameter, proposed by Hansen and O'Leary [21], was proven to produce good regularisation parameters in several cases; however, locating the corner in a robust way is not always an easy task because the L-curve sometimes displays several corners and sometimes the corner is not visible at all. On the contrary, the fixed-point method and its variants [22–24] have been proven to circumvent these difficulties on several test problems.

In the present paper, the Tikhonov regularisation method coupled to the fixed-point method for determining a proper value of the regularisation parameter was adopted to estimate the local convective heat flux at the fluid-wall interface in coiled tubes under the formulation of the linear IHCP in the wall. The temperature distributions on the external wall of the coiled tube, which are acquired using the infrared technique, were adopted as input data of the IHCP in the wall of the tube.

The investigation was particularly focused on the laminar flow regime, which is often found in coiled tube heat-exchanger applications. The purpose of this paper is twofold: to illustrate the estimation technique, which has been originally customised for this specific inverse problem, and to test it on an experimental case. The results, although obtained for a limited range of experimental conditions, are representative of a wide range of technical applications. Moreover, the data could be employed both as a useful benchmark for CFD results as well as in the design of coiled tube heat exchangers for the treatment of highly viscous fluids.

2. Experimental setup and data processing

In the present investigation, a smooth-wall helically coiled stainless steel type AISI 304 tube was tested. It was characterised by eight coils following an helical profile along the axis of the tube where the helix diameter and the pitch were of approximately 310 mm and 200 mm, respectively. The tube internal diameter was 14 mm, and the wall thickness measures 1.0 mm. This geometry yields a coiled pipe length L of approximately 10 m, a dimensionless curvature Γ of 0.045 and a torsion Π of 0.21.

The working fluid was conveyed by a volumetric pump to an holding tank, and it entered the coiled test section equipped with stainless-steel fin electrodes, which were connected to a power supply, type HP 6671A. This setup allowed investigation of the heat transfer performance of the tube under the prescribed condition of uniform heat flux generated by the Joule effect in the wall. The heat

flux provided to the fluid was selected to make the buoyancy forces negligible compared to inertial ones for the fluid velocity values investigated here.

The coiled section was inserted horizontally in a loop completed by a secondary heat exchanger that was fed with city water, which enabled keeping the working fluid temperature constant at the tube inlet.

To minimise the heat exchange with the environment, the heated section was thermally insulated.

A small portion of the external tube wall, near the downstream region of the heated section, was made accessible to an infrared imaging camera by removing the thermally insulating layer, and it was coated by a thin film of opaque paint of uniform and known emissivity.

Therefore, the test section was taken approximately 9 m downstream from the inlet section, in the region of the heated section where, according to [4–6,25], the laminar boundary layers reached the asymptotic profiles. This condition makes the results obtained for this particular section representative of the thermally fully developed region.

The surface temperature distribution was acquired by means of a FLIR SC7000 unit, with a 640 × 512 pixel detector array. Its thermal sensitivity, as reported by the instrument manufacturer, is 20 mK at 303 K, while its accuracy is ±1 K. A sketch of the experimental setup is reported in Fig. 1; Fig. 2 shows the laboratory facility.

To measure the temperature distribution on the whole heat-transfer test section surface, multiples images were acquired, moving the infrared camera around the section. When using an infrared scanner, care should be taken while performing measurements if the scanned surface is not locally normal to the viewed rays due to directional emissivity of the surface.

However, in the present experimental setup, the viewing angle was limited to less than ±30°, and in this condition, the surface was considered to be behaving as a diffuse grey emitter [26]. The effective emissivity of the coating was estimated in situ by shooting a target at different known temperatures [27], and the value 0.99 was found.

The acquired images, thanks to a position reference fixed on the tube wall, were conveniently cropped, processed by perspective algorithms [28] and merged together in Matlab® environment to obtain continuous temperature functions on the tube wall versus the circumferential angular coordinate. Due to the infrared camera set-up adopted in this work (e.g., the focal length and the camera position with respect to the tube test section), temperature values

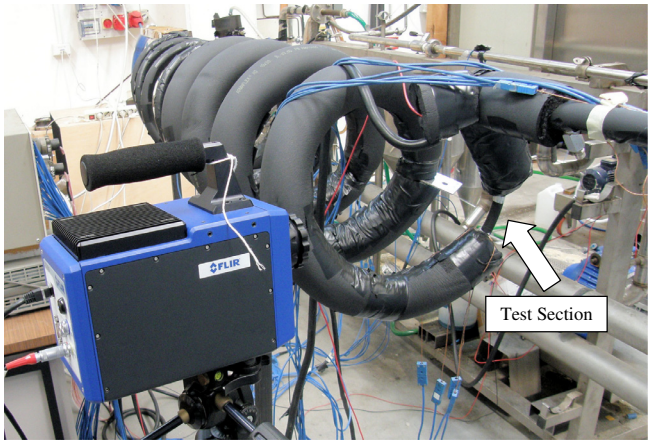

Fig. 2. The experimental facility.

at 256 angular positions over the whole circumferential section were obtained.

The inlet and the outlet fluid bulk temperatures were measured with type-T thermocouples, previously calibrated and connected to a multichannel ice point reference, type KAYE K170-50C. The bulk temperature at any location in the heat transfer section was then calculated from the power supplied to the tube wall. Volumetric flow rates were obtained by measuring the time needed to fill a volumetric flask placed at the outlet of the test section.

The tests were performed by varying the Reynolds number, and consequently the Dean number, which are defined, according to [25] as follows:

$$Re = \frac{\rho_f \cdot w \cdot D_{\text{int}}}{\mu_f}, \tag{1}$$

$$De = Re \cdot \sqrt{\frac{D_{\text{int}}}{a}}, \tag{2}$$

where w is the mean fluid axial velocity, D_{int} is the tube internal diameter, a is the coil diameter, μ_f is the fluid dynamic viscosity and ρ_f is the fluid density, evaluated at the bulk temperature.

To investigate the heat transfer performance of coiled tubes in the laminar flow regime, ethylene glycol was used as the working

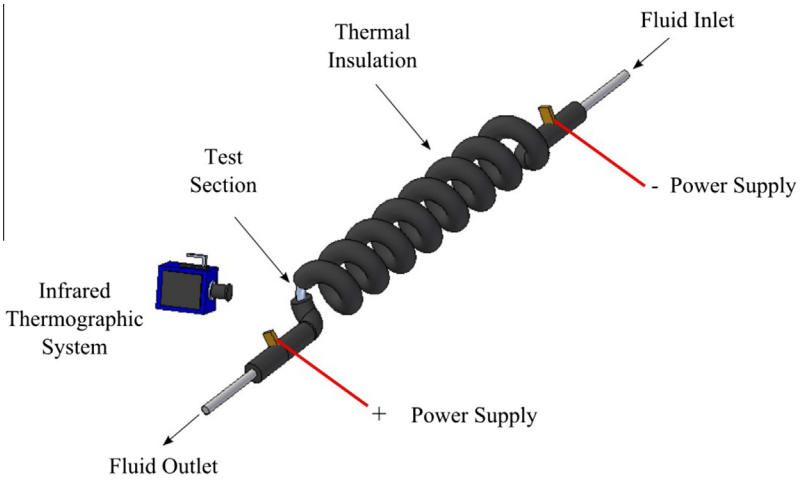

Fig. 1. Sketch of the experimental setup.

fluid in the Reynolds number range 135−1050. In the temperature range characterising the experimental conditions, the Prandtl number of the working fluid varied in the range of 170–200.

3. Estimation procedure

The description of the estimation procedure starts with the modelling of the direct heat-transfer problem, proceeds by applying the Tikhonov regularisation method with the support of the fixed-point iteration technique and concludes with the estimation of the local convective heat-transfer coefficient.

3.1. Numerical model

The simplified 2-D model of the test section (sketched in Fig. 3) was formulated by assuming that the temperature gradient is almost negligible along the axis of the tube.

In the 2-D solid domain, the steady-state energy balance equation is expressed in the (r, α) coordinate system in the form:

$$\frac{k}{r}\frac{\partial}{\partial r}\left(r\frac{\partial T}{\partial r}\right)+\frac{k}{r^2}\frac{\partial^2 T}{\partial \alpha^2}+q_g=0, \tag{3}$$

where q_g is the heat generated by the Joule effect in the wall, k is the wall thermal conductivity and α is the angular coordinate, [29].

The following two boundary conditions completed the energy balance equation:

$$k\frac{\partial T}{\partial r}=\frac{(T_{env}-T)}{R_{env}}, \tag{4}$$

which is applied on surface S_1 and where R_{env} is the overall heat-transfer resistance between the tube wall and the surrounding environment with temperature T_{env};

$$-k\frac{\partial T}{\partial r}=q(\alpha), \tag{5}$$

which is applied on surface S_2 and where q is the local convective heat flux at the fluid-internal wall interface, assumed to be varying with the angular coordinate α.

To express the problem in the discrete domain, the convective heat flux distribution can be simplified by considering that it is described by a continuous, piecewise linear function composed of p sections as follows:

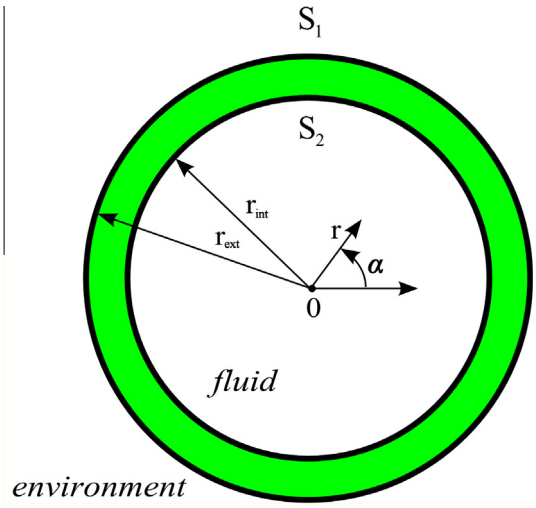

Fig. 3. Geometrical domain with a coordinate system.

$$q(\alpha)=\begin{cases} b_p+\alpha\cdot\left(\frac{b_1-b_p}{2\pi/p}\right), & 0\le\alpha<\frac{1\cdot 2\pi}{p}\\ b_1+\alpha\cdot\left(\frac{b_2-b_1}{2\pi/p}\right), & \frac{1\cdot 2\pi}{p}\le\alpha<\frac{2\cdot 2\pi}{p}\\ \dots\\ b_{m-1}+\alpha\cdot\left(\frac{b_{m+1}-b_m}{2\pi/p}\right), & \frac{m\cdot 2\pi}{p}\le\alpha<\frac{(m+1)\cdot 2\pi}{p}\\ \dots\\ b_{p-2}+\alpha\cdot\left(\frac{b_{p-1}-b_{p-2}}{2\pi/p}\right), & \frac{(p-2)\cdot 2\pi}{p}\le\alpha<\frac{(p-1)\cdot 2\pi}{p}\\ b_{p-1}+\alpha\cdot\left(\frac{b_p-b_{p-1}}{2\pi/p}\right), & \frac{(p-1)\cdot 2\pi}{p}\le\alpha<\frac{p\cdot 2\pi}{p} \end{cases} \tag{6}$$

As suggested by Beck et al. [12] and Dennis et al. [30], because the problem is linear with respect to the heat flux $q(\alpha)$, it can be written in the discrete domain as follows:

$$\mathbf{T}=\mathbf{X}\mathbf{q}+\mathbf{T}_{\mathbf{q}=0}, \tag{7}$$

where $\mathbf{T}$ is the vector of the discrete temperature data at the external coil surface, $\mathbf{q}$ is the heat flux vector at the fluid-internal wall interface, $\mathbf{T_{q=0}}$ is a constant term and $\mathbf{X}$ is the sensitivity matrix.

The heat-flux vector $\mathbf{q}$ is a column vector composed by $b_1, b_2, \dots, b_p$ values.

The sensitivity matrix $\mathbf{X}$ values were calculated using the two-point difference approach:

$$X_{i,j}=\frac{T_i(q_1,q_2,\dots,q_j+\Delta q,\dots,q_n)-T_i(q_1,q_2,\dots,q_j,\dots,q_n)}{\Delta q} \tag{8}$$

where T_i is the temperature value at the i sensor position obtained by solving Eqs. (3)–(5)and imposing an internal heat flux distribution as defined by Eq. (6).

In an analogous way, the constant vector was determined by imposing a null heat flux:

$$T_{q=0,i}=T_i(q_1=0,q_2=0,\dots,q_j=0,\dots,q_n=0). \tag{9}$$

The direct formulation of the problem is concerned with the determination of the temperature distribution on the tube external wall when the convective heat flux vector $\mathbf{q}$ is known. In the inverse formulation considered here, $\mathbf{q}$ is instead regarded as being unknown, whereas the surface temperature is measured.

3.2. Tikhonov regularisation method

The function estimation procedure is embedded in the inverse solution of the problem expressed by Eq. (7). The temperature distribution on the external surface of the section, $\mathbf{T}$, can be easily computed numerically, by imposing a trial convective heat flux distribution on the internal wall side $\mathbf{q}$.

Observing Eq. (7), it must be highlighted that the constant term $\mathbf{T_{q=0}}$ and the sensitivity matrix $\mathbf{X}$ are not functions of the unknown variable $\mathbf{q}$, and this fact confirms that the inverse heat conduction problem investigated here is linear.

In the inverse formulation, this computed temperature distribution $\mathbf{T}$ is forced to match the experimental temperature distribution $\mathbf{Y}$, by tuning the convective heat-flux distribution on the internal wall side $\mathbf{q}$. The matching of the two temperature distributions (the computed and the experimentally acquired) could be easily performed under a least square approach. However, due to the ill-posed nature of the problem, the least square solution is generally dominated by noise, and some type of regularisation is required. As mentioned before, in this work the Tikhonov regularisation method is adopted; this approach, successfully applied in the inverse heat-transfer literature [30–36], makes it possible to reformulate the original problem as a well-posed problem that consists of minimising the following objective function:

$$J(\mathbf{q})=\|\mathbf{Y}-\mathbf{X}\mathbf{q}-\mathbf{T}_{\mathbf{q}=0}\|_2^2+\lambda^2\|\mathbf{L}\mathbf{q}\|_2^2,\quad \lambda>0, \tag{10}$$

where $\|\cdot\|_2^2$ stands for the square of the 2-norm, λ is the regularisation parameter, **L** is the derivative operator and **T** is the distribution of the external surface temperature derived from a direct numerical solution of the problem obtained by imposing a given convective heat flux distribution on the internal wall side **q**. Often, **L** is the zero, first or second derivative operator: in this work the second-order derivative formulation was chosen to preserve the local variation in the heat-flux distribution.

Minimisation of **J**(**q**) is equivalent to solving the regularised normal equations [34]:

$$(\mathbf{X}^t\mathbf{X} + \lambda^2\mathbf{L}^t\mathbf{L})\mathbf{q} = \mathbf{X}^t(\mathbf{Y} - \mathbf{T}_{\mathbf{q}=0}), \lambda > 0, \tag{11}$$

whose solution is unique when the null spaces of matrices **X** and **L** intersect trivially. Here, superscript *t* stands for matrix transposition. This solution, often referred to as the regularised solution, can therefore be expressed as:

$$\mathbf{q}_\lambda = (\mathbf{X}^t\mathbf{X} + \lambda^2\mathbf{L}^t\mathbf{L})^{-1}\mathbf{X}^t(\mathbf{Y} - \mathbf{T}_{\mathbf{q}=0}), \lambda > 0 \tag{12}$$

In practice, $\mathbf{q}_\lambda$ can be computed efficiently using standard linear algebra tools such as the Cholesky decomposition of matrix $\begin{pmatrix}\mathbf{X}\\ \lambda\mathbf{L}\end{pmatrix}$ or the generalised singular value decomposition (GSVD) of the matrix pair (**X**,**L**) [34].

The function expressed in Eq. (10) represents a trade-off between two optimisation processes: first, the fidelity of the fit and second, the smoothness or the stability of the solution. Thus, an appropriate choice of λ should give an optimal balance, which in turn, should lead to a reliable approximation of the wanted solution.

3.3. Regularisation parameter

The importance of the choice of the regularisation parameter has been widely analysed in the literature.

For a survey of the Tikhonov parameter choice rules the reader is referred to Hansen [34]. Choosing a large regularisation parameter means that imposing too much regularisation on the solution prejudices the fitting of the data and the ability to obtain a great residual; the absence of regularisation or an insufficiently small regularisation parameter will provide a good fitting but also a solution affected by data errors. Therefore, the choice of a proper regularisation parameter requires a good balance between the size of the residual norm and the size of the solution norm (semi norm); this is what motivated the development of the L-curve method proposed by Hansen and O'Leary [21]. This method determines the regularisation parameter by locating the 'corner' of the parametric curve in the **u**, **v** plane defined by:

$$\begin{cases}\mathbf{u}_\lambda = \log(\|\mathbf{Y} - \mathbf{X}\mathbf{q}_\lambda - \mathbf{T}_{\mathbf{q}=0}\|_2)\\ \mathbf{v}_\lambda = \log(\|\mathbf{L}\mathbf{q}_\lambda\|_2)\\ \lambda > 0\end{cases} \tag{13}$$

The motivation for this choice of the regularisation parameter is that very often this curve is L-shaped, and its corner corresponds to a parameter that produces a good balance between the residual norm and the solution norm. From a computational point of view, the 'corner' is taken to be the point on the L-curve where the curvature is maximised; see Hansen and O'Leary [21]. In practice, the L-curve method has been proven to produce good regularisation parameters in several cases. However, locating the corner in a robust way is not always an easy task, either because sometimes the curve displays several corners or because the corner is not visible at all. A method that has been proven to circumvent the difficulties of the L-curve method on several test problems from the literature is the fixed-point method and its variants proposed by Bazán and co-workers [22–24]. The fixed-point method requires the computation of the solution seminorm and the corresponding residual norm, and it selects the parameter that minimises the product of these norms as a function of the regularisation parameter. Like the L-curve, the motivation to use this algorithm is that the sought minimiser corresponds to a good balance between the size of these norms. Algorithmically, the regularisation parameter chosen by the fixed-point method is the limit value of the sequence:

$$\lambda_{k+1} = \varphi(\lambda_k) = \frac{\|\mathbf{Y} - \mathbf{X}\mathbf{q}_{\lambda_k} - \mathbf{T}_{\mathbf{q}=0}\|_2}{\|\mathbf{L}\mathbf{q}_{\lambda_k}\|_2}, k = 0, 1, 2, \ldots \tag{14}$$

The value for the regularisation parameter can also be visually represented as a fixed-point of the curve.

In practice, the sequence converges very quickly, and the computed regularisation parameter yields solutions with accuracy comparable to that of the L-curve method, but it is more robust and less computationally expensive [22–23]. Like the L-curve approach, the fixed-point method does not require *a priori* knowledge of the noise level.

In this work, the regularised solution $\mathbf{q}_\lambda$ is computed efficiently by means of the GSVD of the matrix pair (**X**,**L**), which simplifies enormously the implementation of the fixed-point algorithm; for the algorithmic details and the stopping criterion of the sequence (14), the reader is referred to Bazán [22].

3.4. Heat transfer characterisation

Once the heat-flux distribution at the fluid-wall interface compatible with the experimental temperature data has been determined through the strategy described above, the local convective heat-transfer coefficient can be easily determined, as follows:

$$h_{\text{int}}(\alpha) = \frac{q_\lambda(\alpha)}{T(\alpha, r = r_{\text{int}}) - T_b}, \tag{15}$$

where $q_\lambda(\alpha)$ is the heat flux distribution estimated under the solution approach based on the Tikhonov regularisation method with the support of fixed-point iteration techniques, T_b is the bulk-fluid temperature on the test section, calculated from the energy balance on the heated section as described in [4–6] and $T(\alpha, r = r_{int})$ is temperature distribution on the tube internal wall efficiently estimated by numerically solving the direct problem expressed by Eqs. (3)–(5)by imposing a convective heat flux equal to $q_\lambda(\alpha)$.

The convective heat transfer coefficient can be suitably expressed in a dimensionless form by means of the local Nusselt number, as follows:

$$Nu = \frac{h_{\text{int}} \cdot D_{\text{int}}}{k_f}, \tag{16}$$

where k_f is the fluid thermal conductivity, evaluated at the bulk temperature.

For each dataset, the average Nusselt number value was also determined as follows:

$$Nu_{avg} = \frac{\int_{\alpha=0}^{2\pi} q(\alpha) \cdot d\alpha}{\overline{T_w} - T_b} \cdot \frac{D_{\text{int}}}{k_f}, \tag{17}$$

where

$$\overline{T_w} = \frac{\int_{\alpha=0}^{2\pi} T(\alpha, r = r_{\text{int}}) \cdot d\alpha}{2\pi}. \tag{18}$$

The accuracy associated with the estimated values was assigned by the parametric bootstrap method [35,37,38]: the input data of the estimation procedure are re-sampled from their respective probability distributions and, from these values, the unknowns are calculated by the estimation procedure presented above; this process is repeated many times, and the results are processed using standard statistical techniques for evaluating 95% confidence intervals.

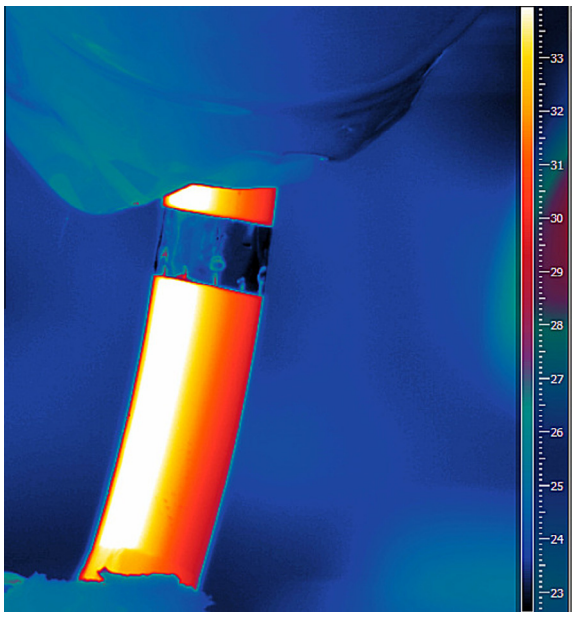

Fig. 4. Representative infrared image of the coil wall (Re = 558, Pr = 182).

4. Results

A representative temperature map acquired by the infrared camera is reported in Fig. 4. The data clearly reveal that the temperature distribution exhibits a significant variation along the circumference, and the temperature gradient is almost negligible along the axis of the tube. This observation confirms that adopting a 2-D numerical model for this type of problem is appropriate.

The corresponding temperature distribution over the whole wall circumference is reported in Fig. 5, where the angular coordinate origin was taken at the inner side of the coil.

To express the direct problem in the discrete domain, the convective heat-flux distribution was simplified here by considering the function expressed by Eq. (6) with p equal to 36. Adopting a point every 10 angular degrees for the convective heat flux distribution represents a good compromise between model precision and the computational cost. Moreover, it must be noted that the linear formulation of the IHCP makes it possible to increase the number of degrees of freedom of the problem with respect to previous investigations [10] by making it feasible to appreciate the local variations in the convective heat-transfer-coefficient distribution.

To calculate the $\mathbf{T_{q=0}}$ and $\mathbf{X}$ terms of Eq. (7), the numerical solution of Eq. (3)–(5)was calculated by the finite element method implemented in Comsol Multiphysics® environment with a mesh of approximately 2596 triangular elements. The overall heat-transfer resistance between the tube wall and the surrounding environment R_{env}, which was assumed to be known in the inverse problem considered here, was taken equal to 0.2 m^2 K/W, which is a representative value for natural convection in air compounded with radiative heat transfer with the environment. The wall thermal conductivity k was certified by the manufacturer equal to 15 W/m K; the heat generated by the Joule effect in the wall q_g was calculated by the ratio of the power supplied and the volume of the tube wall.

The method proposed by Hansen and O'Leary [21], based on the curvature of the L-curve, was applied to the present data without success. The L-curve, shown in Fig. 6, displays more than one 'corner', making the determination of a proper regularisation parameter unfeasible in this approach. To overcome this, the fixed-point method was employed, as shown in Fig. 7. The analysis reveals that a proper λ value is equal to $1.17 \cdot 10^{-5}$.

In Fig. 8, the reconstructed temperature distribution for λ equal to $1.17 \cdot 10^{-5}$ is compared to the experimental data. Fig. 9 shows that the residuals between the experimental and the computed temperature values are randomly distributed. This confirms that the simplified numerical model used in this study adequately describes the physical problem being tested [12]. The residual norm is equal to 0.59 K, and it is larger than the noise level, quantified to approximately 0.04 K. The noise level has been measured by measuring the surface temperature distribution while maintaining the coil wall under isothermal conditions. This evidence confirms the observation of the properties of the fixed-point method, as illustrated by Bazán [22].

The distribution of the convective heat flux restored by the minimisation procedure presented above is reported in Fig. 10. As expected, the convective heat flux between the tube wall and the fluid is minimal close to the inner bend side.

A mesh refinement study was conducted to verify the appropriateness of the mesh size of the finite element model in relation to the inverse problem solution. Table 1 compares the results, reported in terms of the higher and the lower heat flux values at different mesh distributions, and it confirms that the adopted mesh ensures a satisfactory solution.

The 95% confidence interval associated with the estimated heat flux was determined by parametric bootstrap [35,37,38], assuming

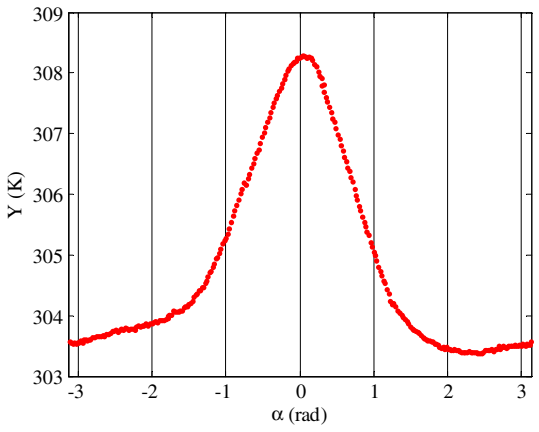

Fig. 5. Temperature distribution on the coil external wall (Re = 558, Pr = 182).

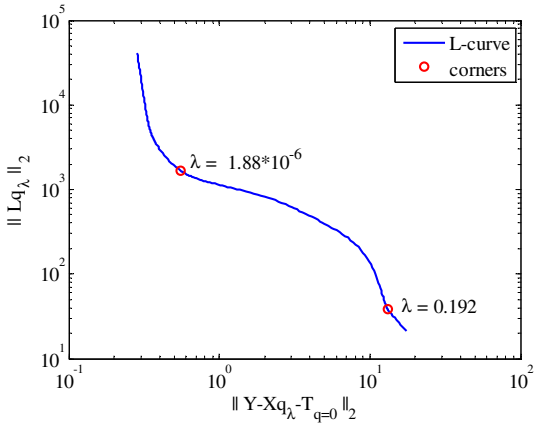

Fig. 6. L-curve in log–log scale and points of its maximal curvature (Re = 558, Pr = 182).

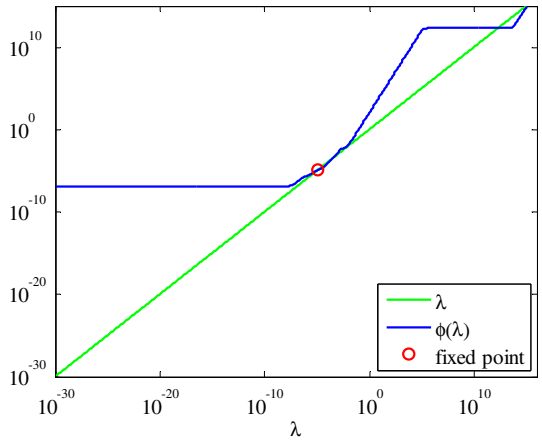

Fig. 7. Fixed-point analysis (Re = 558, Pr = 182).

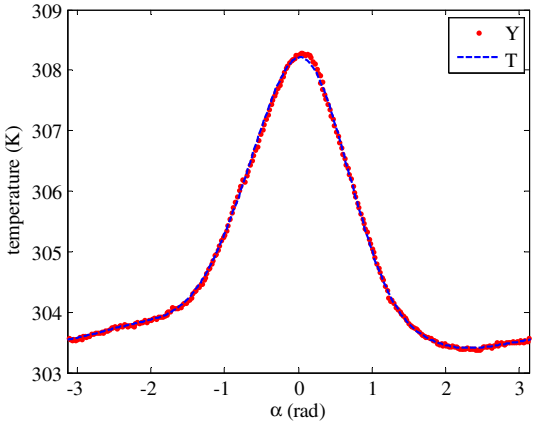

Fig. 8. Experimental (Y) and reconstructed (T) temperature distribution ($\lambda = 1.17 \cdot 10^5$, Re = 558, Pr = 182).

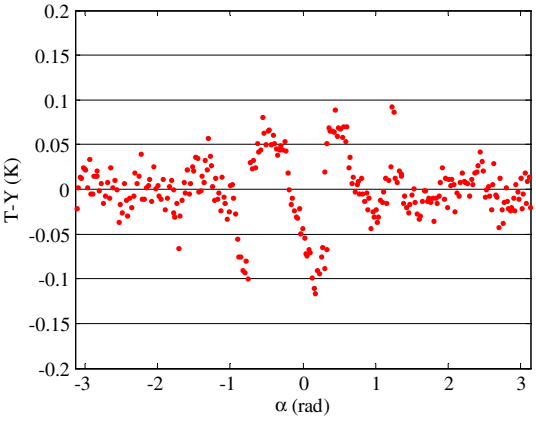

Fig. 9. Residuals between the experimental and the reconstructed temperature distribution ($\lambda = 1.17 \cdot 10^{-5}$, Re = 558, Pr = 182).

the uncertainties in the input data reported in Table 1. The estimated confidence interval for this experimental run is approximately ±170 W/m^2.

To identify the main contributions to the uncertainty of the estimated heat flux distribution, the influence coefficient values [39] were calculated:

$$J_\xi^Z = \left(\frac{\partial Z}{\partial \xi} w_\xi\right)^2, \tag{19}$$

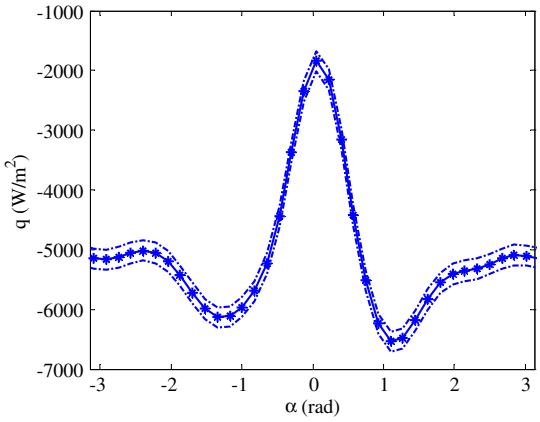

Fig. 10. Restored convective heat-flux distribution with a 95% confidence interval ($\lambda = 1.17 \cdot 10^{-5}$, Re = 558, Pr = 182).

Table 1
Mesh refinement study (Re = 558).

No. of elements	1298	2596	5144
q_{max} (W/m^2)	6534.1	6534.1	6534.1
q_{min} (W/m^2)	1843.0	1842.9	1842.9
q_{max}/q_{min}	3.5454	3.5456	3.5456

Table 2
The 95% confidence interval of the main physical quantities involved in the estimation procedure.

Y (K)	α (°)	k (W/m K)	T_{env} (K)	R_{env} (m^2 K/W)	q_g (W/m^3)	T_b (K)
±0.1 K	±4°	±5%	±0.1 K	±50%	±4%	±0.1 K

where Z is the estimated quantity and ξ is the considered input parameter with an uncertainty equal to w_ξ.

For the inverse problem investigated in this paper, the analytical determination of the partial derivative present in Eq. (19) is impossible, and the adoption of a finite difference approach is needed: (Table 2)

$$\frac{\partial Z}{\partial \xi} \cong \frac{Z(\xi + \Delta\xi) - Z(\xi)}{\Delta\xi}, \tag{20}$$

where $\Delta\xi$ is a small variation of the input parameter ξ.

Table 3 reports the influence-coefficient values for the main input parameters, considering the maximum and the minimum of the estimated heat flux as representative output quantities of the inverse problem solution. These results underline that the main contributions to the uncertainty are the k and q_g measurements, and the uncertainties in R_{env} and T_{env} are almost insignificant. This means that the heat exchanged between the tube wall and the environment is negligible in comparison to that exchanged between the tube wall and the working fluid. On the contrary, to improve the overall situation, particular attention to the accuracy of k and q_g should be given.

The resulting distribution of the convective heat transfer coefficient at the fluid–wall interface according to Eq. (15) is reported in Fig. 11. The variation in the convective heat transfer coefficient along the boundary of the duct section indicates that in the fully developed heat transfer region, h_{int} is minimal close to the inner bend side of the coil, and it reaches its maximum at the outer bend side due the onset of the secondary flows [3,7,8] induced by the wall curvature.

Table 3
Influence coefficient values of k, T_{env}, R_{env} and q_g on the maximum and the minimum of the estimated heat-flux distribution.

	k	T_{env}	R_{env}	q_g
q_{max}	$J_k^{q_{max}} = 5.3 \cdot 10^3$ W^2/m^4	$J_{T_{env}}^{q_{max}} = 0.33$ W^2/m^4	$J_{R_{env}}^{q_{max}} = 3.8 \cdot 10^2$ W^2/m^4	$J_{q_g}^{q_{max}} = 4.2 \cdot 10^4$ W^2/m^4
q_{min}	$J_k^{q_{min}} = 2.6 \cdot 10^4$ W^2/m^4	$J_{T_{env}}^{q_{min}} = 0.33$ W^2/m^4	$J_{R_{env}}^{q_{min}} = 8.4 \cdot 10^2$ W^2/m^4	$J_{q_g}^{q_{min}} = 5.1 \cdot 10^3$ W^2/m^4

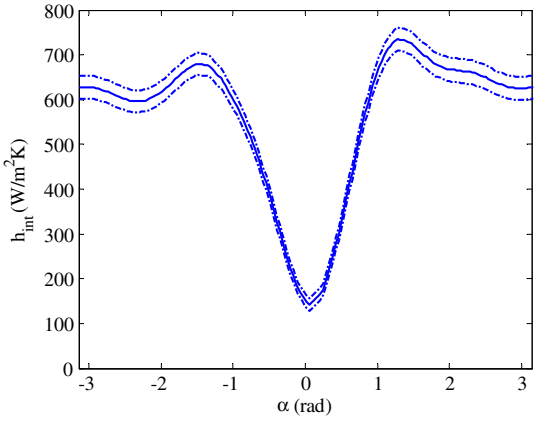

Fig. 11. Restored convective heat-transfer coefficient distribution with 95% confidence interval ($\lambda = 1.17 \cdot 10^{-5}$, $Re = 558$, $Pr = 182$).

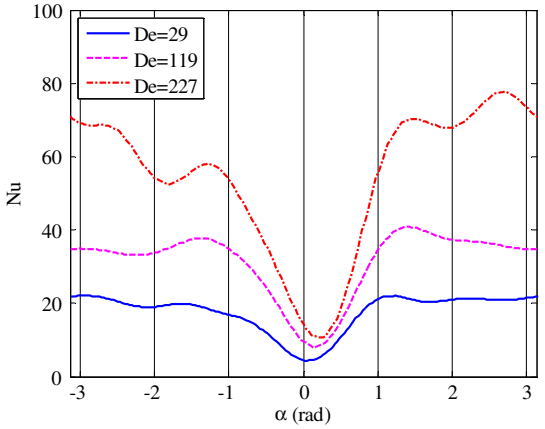

Fig. 12. Restored Nusselt number distribution for three representative Dean number values.

The entire estimation procedure was repeated for various Reynolds number values: the experimental conditions are reported in Table 4, and representative results are plotted in Fig. 12.

To verify if free convection effects are relevant with respect to forced convection effects, the ratio Gr/Re^2 was evaluated, where Gr and Re are the Grashof and the Reynolds numbers, respectively [29].

The value of this ratio for the present experimental conditions is specified in Table 4. Being $Gr/Re^2 \ll 1$ for all the runs, the gravity effects can be considered negligible if compared to the inertial ones and this makes the measurements taken in a single section representative of the thermally developed conditions for the forced convection flows.

The data clearly show the effect of torsion induced by the coil pitch: it creates a rotation force that affects the flow pattern. Consequentially, it makes the distribution of the Nusselt number non-symmetrical, as already observed by Yang et al. [7]: the heat-transfer rate is increased on half of the tube wall compared to that on the other half. Moreover, as the Dean number increases, the location of the minimum Nusselt number shifts slightly from zero to higher angular coordinate values: the minimum is at approximately $\alpha = 0.02$ for De equal to 29, and it is at $\alpha = 0.15$ for De equal to 227.

Table 4
Experimental conditions.

Re	Pr	q_g (W/m^3)	T_b (K)	$\overline{T_w}$ (K)	Gr/Re^2
135	172	$2.7 \cdot 10^6$	296.6	305.9	$3.4 \cdot 10^{-2}$
375	174	$4.8 \cdot 10^6$	296.4	307.1	$5.0 \cdot 10^{-2}$
465	163	$4.8 \cdot 10^6$	298.0	306.5	$2.9 \cdot 10^{-2}$
558	182	$4.8 \cdot 10^6$	295.2	304.7	$1.8 \cdot 10^{-3}$
665	185	$4.8 \cdot 10^6$	294.7	303.4	$1.1 \cdot 10^{-3}$
703	187	$4.8 \cdot 10^6$	294.5	302.4	$9.1 \cdot 10^{-4}$
904	189	$4.8 \cdot 10^6$	294.1	300.3	$4.2 \cdot 10^{-4}$
1006	190	$4.8 \cdot 10^6$	293.9	299.5	$3.0 \cdot 10^{-4}$
1060	196	$4.8 \cdot 10^6$	293.1	299.0	$2.7 \cdot 10^{-4}$
1098	175	$4.8 \cdot 10^6$	296.2	300.3	$2.2 \cdot 10^{-4}$

To locally compare the Nusselt distributions estimated for the various De values, the shifting effect of the torsion was compensated by introducing a relative angle α^* into the analysis, whose origin was taken where the Nusselt number reaches its minimum.

Fig. 13 reports the Nu/Nu_{max} ratio for various Dean numbers: by accounting for the experimental uncertainty, it can be stated that this ratio is almost independent of the Dean number. A similar observation was made by Jayakumar et al. [8] for turbulent heat transfer in helical pipes.

Moreover, the data show that, at the outside surface of the coil, the Nusselt number is approximately five times that at the inside surface. The pattern is particularly steep and Nu/Nu_{max} is above 0.8 for approximately 75% of the circumference.

Fig. 14 reports the best fit of the experimental distributions reported in Fig. 13, along with the 95% confidence interval and the correlations found by Yang et al. [7] and Bozzoli et al. [10]. The asymmetric profile of the curve clearly shows the effect of the torsion induced by the coil pitch: the heat-transfer rate is increased on half of the tube wall ($0 < \alpha^* < \pi$) compared to that on the other

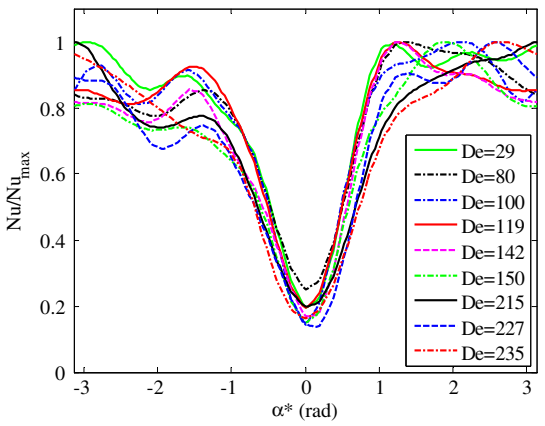

Fig. 13. Normalised local Nusselt number for various Dean numbers.

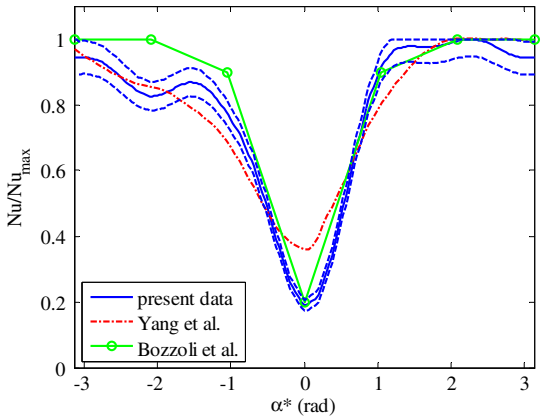

Fig. 14. Normalised local Nusselt number and comparison with the data by Yang et al. [7] and Bozzoli et al. [10].

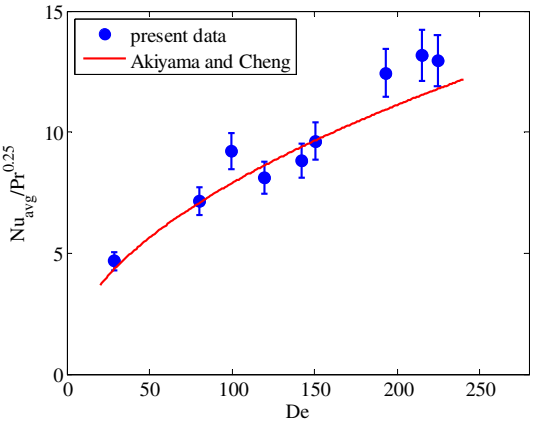

Fig. 15. Average Nusselt number values compared with the correlation by Akiyama and Chen [40].

half ($-\pi < \alpha^* < 0$), as already numerically observed by Yang et al. [7] (see Fig. 14).

A good agreement between the Nu/Nu_{max} correlation found here and the one proposed by Bozzoli et al. [10] was observed, although the latter suffers from a few limitations due to several strong approximations in the model formulation.

The data by Yang et al. [7] mainly match the distribution obtained here, although some discrepancies are registered, especially close to the inner bend side of the coil. This may be because Yang et al. [7] derived their data for a coiled tube with a torsion value similar to the one of the tube investigated here but for a fluid with a Prandtl number equal to 5.

The circumferential average of the Nusselt number values, determined according to Eq. (17), is in substantial agreement with the correlation proposed by Akiyama and Cheng [40] for smooth-wall coiled tubes (see Fig. 15).

5. Conclusions

In this paper, a procedure to estimate the local convective heat transfer coefficient in coiled tubes is presented and tested. The investigation was focused on the fully developed region for the laminar flow regime in the Reynolds number range of 135–1050 and the Prandtl number range of 170–200.

The temperature distribution maps on the external coil wall are employed as input data of the linear inverse heat conduction problem in the wall under a solution approach based on the Tikhonov regularisation method with the support of the fixed-point iteration technique to determine the proper regularisation parameter.

The linear formulation of the inverse heat conduction problem makes it possible to increase the number of degrees of freedom of the problem with respect to previous investigations [10], thereby allowing better appreciation of local variations in the distribution of the convective heat-transfer coefficient. The application of the fixed-point iteration technique circumvented the difficulties of the classical L-curve method to determine a proper regularisation parameter.

The results, reported with their 95% confidence interval, showed that the variation in the convective heat transfer coefficient along the boundary of the duct section is very significant: at the outside surface of the coil, the Nusselt number is approximately five times larger than that at the inside surface.

Although the data used in this study have been obtained for a limited range of experimental conditions, we emphasise that they are representative of a wide range of technical applications. Moreover, because in the scientific literature there is a lack of knowledge about the local heat-transfer coefficient for the laminar flow regime in coiled tubes, the results obtained here might be particularly useful in the validation of numerical models and in the design of coiled tube heat exchangers aimed at the treatment of highly viscous fluids. The extension of this investigation to other tube geometries, fluids and types of flow will be the subject of future works.

Acknowledgements

This work was partially supported by the Emilia-Romagna Region (POR FSE 2007–2013). MBS srl (Parma, Italy) is gratefully acknowledged for the set-up of the experimental apparatus.

The work of the fourth author is supported by CNPq, Brazil, grants 308709/2011-0, 477093/2011-6.

The authors thank Prof. Giorgio Pagliarini for the helpful and valuable discussion of the results presented here.

References

[1] A. Zachár, Analysis of coiled-tube heat exchangers to improve heat transfer rate with spirally corrugated wall, Int. J. Heat Mass Transfer 53 (2010) 3928–3939.
[2] I. Di Piazza, M. Ciofalo, Numerical prediction of turbulent flow and heat transfer in helically coiled pipes, Int. J. Therm. Sci. 49 (4) (2010) 653–663.
[3] S. Rainieri, F. Bozzoli, L. Schiavi, G. Pagliarini, Numerical analysis of convective heat transfer enhancement in swirl tubes, Int. J. Numer. Meth. Heat Fluid Flow 21 (5) (2011) 559–571.
[4] S. Rainieri, F. Bozzoli, L. Cattani, G. Pagliarini, Experimental investigation on the convective heat transfer enhancement for highly viscous fluids in helical coiled corrugated tubes, J. Phys.: Conf. Ser. 395 (2012), Paper No. 012032.
[5] S. Rainieri, F. Bozzoli, G. Pagliarini, Experimental investigation on the convective heat transfer in straight and coiled corrugated tubes for highly viscous fluids: Preliminary results, Int. J. Heat Mass Transfer 55 (1–3) (2012) 498–504.
[6] S. Rainieri, F. Bozzoli, L. Cattani, G. Pagliarini, Compound convective heat transfer enhancement in helically coiled wall corrugated tubes, Int. J. Heat Mass Transfer 59 (2013) 353–362.
[7] G. Yang, F. Dong, M.A. Ebadian, Laminar forced convection in a helicoidal pipe with finite pitch, Int. J. Heat Mass Transfer 38 (5) (1995) 853–862.
[8] J.S. Jayakumar, S.M. Mahajani, J.C. Mandal, N.I. Kannan, P.K. Vijayan, CFD analysis of single-phase flows inside helically coiled tubes, Comput. Chem. Eng. 34 (2010) 430–446.
[9] B. Bai, L. Guo, Z. Feng, X. Chen, Turbulent heat transfer in a horizontal helically coiled tube, Heat Transfer-Asian Res. 28 (5) (1999) 395–403.
[10] F. Bozzoli, L. Cattani, S. Rainieri, G. Pagliarini, Estimation of local heat transfer coefficient in coiled tubes under inverse heat conduction problem approach, Exp. Therm. Fluid Sci. (2013), http://dx.doi.org/10.1016/j.expthermflusci.2013.11.024.
[11] J.V. Beck, K. Arnold, Parameter Estimation in Engineering and Science, Wiley Interscience, New York, 1977.
[12] J.V. Beck, B. Balckwell, Jr C.R. St.Clair, Inverse Heat Conduction – Ill-posed problems, John Wiley & Sons Inc., New York, 1985.
[13] O.M. Alifanov, Inverse Heat Transfer Problem, Springer, Berlin, 1994.

[14] H.R.B. Orlande, O. Fudym, D. Maillet, Thermal Measurements and Inverse Techniques, CRC Press, Taylor & Francis Group, Boca Raton, 2011.
[15] O.M. Alifanov, Solution of an inverse problem of heat conduction by iteration methods, J. Eng. Phys. 26 (4) (1974) 471–476.
[16] D.A. Murio, The Mollification Method and the Numerical Solution of Ill-Posed Problems, John Wiley and Sons, New York, 1993.
[17] F. Bozzoli, G. Pagliarini, S. Rainieri, Experimental validation of the filtering technique approach applied to the restoration of the heat source field, Exp. Therm. Fluid Sci. 44 (2013) 858–867.
[18] H. Massard, H.R.B. Orlande, O. Fudym, Estimation of position-dependent transient heat source with the Kalman filter, Inverse Probl. Sci. Eng. 20 (7) (2012) 1079–1099.
[19] S.K. Kim, W.I. Lee, Solution of inverse heat conduction problems using maximum entropy method, Int. J. Heat Mass Transfer 45 (2002) 381–391.
[20] A.N. Tichonov, V.Y. Arsenin, Solution of Ill-posed Problems, Winston & Sons, Washington, 1977.
[21] P.C. Hansen, D. O'Leary, The use of the L-curve in the regularization of discrete ill-posed problems, SIAM J. Scient. Comput. 14 (1993) 1487–1503.
[22] F.S.V. Bazán, Fixed-point iteration in determining the Tikhonov regularization parameter, Inverse Probl. Sci. Eng. 24 (2008) 035001.
[23] F.S.V. Bazán, J.B. Francisco, An improved fixed-point algorithm for determining a Tikhonov regularization parameter, Inverse Probl. Sci. Eng. 25 (2009) 045007.
[24] F.S.V. Bazan, L.S. Borges, GKB-FP: an algorithm for large-scale discrete ill-posed problems, Bit Numer. Math. 50 (3) (2010) 481–507.
[25] L.A.M. Janssen, C.J. Hoogendoorn, Laminar convective heat transfer in helical coiled tubes, Int. J. Heat Mass Transfer 21 (1978) 1197–1206.
[26] T. Astarita, G.M. Carlomagno, Infrared Thermography for Thermo-fluid-dynamics, Springer, Berlin, 2012.
[27] S. Rainieri, F. Bozzoli, G. Pagliarini, Characterization of an uncooled infrared thermographic system suitable for the solution of the 2-D inverse heat conduction problem, Exp. Therm. Fluid Sci. 32 (8) (2008) 1492–1498.
[28] B. Cyganek, J.P. Siebert, An Introduction to 3D Computer Vision Techniques and Algorithms, Wiley, New York, 2011.
[29] F.P. Incropera, D. Dewitt, Fundamentals of Heat and Mass Transfer, John Wiley & Sons Inc., New York, 2006.
[30] B.H. Dennis, G.S. Dulikravich, Inverse determination of unsteady temperatures and heat fluxes on inaccessible boundaries, J. Inverse Ill-posed Probl. 20 (5–6) (2013) 791–803.
[31] M.S. Gadala, F. Xu, An FE-based sequential inverse algorithm for heat flux calculation during impingement water cooling, Int. J. Numer. Meth. Heat Fluid Flow 16 (3) (2006) 356–385.
[32] M. Gonzalez, M.B. Goldschmit, Inverse geometry heat transfer problem based on a radial basis functions geometry representation, Int. J. Numer. Meth. Eng. 65 (8) (2004) 1243–1268.
[33] K. Okamoto, B.Q. Li, Optimal Numerical methods for Choosing an Optimal Regularization Parameter, Numer. Heat Transfer Part B: Fundam. 51 (6) (2007) 515–533.
[34] P.C. Hansen, Rank-deficient and Discrete Ill-posed Problems, SIAM, Philadelphia, 1998.
[35] H.R.B. Orlande, F. Olivier, D. Maillet, R.M. Cotta, Thermal Measurements and Inverse Techniques, Taylor and Francis, New York, 2011.
[36] H.J. Reinhardt, D.H. Hào, J. Frohne, F.T. Suttmeier, Numerical solution of inverse heat conduction problems in two spatial dimensions, J. Inverse Ill-Posed Probl. 15 (2007) 19–36.
[37] B. Efron, The Jackknife, the Bootstrap and Other Resampling Plans, Society of Industrial and Applied Mathematics CBMS-NSF Monographs, Philadelphia, 1982.
[38] B. Blackwell, J.V. Beck, A technique for uncertainty analysis for inverse heat conduction problems, Int. J. Heat Mass Transfer 53 (4) (2010) 753–759.
[39] J.P. Holman, Experimental Methods for Engineers-7/E, McGraw-Hill, 2001.
[40] A. Mitsunobu, K.C. Cheng, Boundary vorticity method for laminar forced convection heat transfer in curved pipes, Int. J. Heat Mass Transfer 14 (10) (1971) 1659–1675.